Wind-Tunnel Simulation of Ablation

B.J. Griffith,* E.E. Edenfield,† and W.T. Strike‡
ARO, Inc., Arnold Air Force Station, Tenn.

A comprehensive experimental and theoretical investigation was conducted in Arnold Engineering Development Center (AEDC) tunnel C at Mach number 10 on a sharp 5° half-angle cone in order to study ablation effects under laminar flow conditions. Attention was focused on 1) the mode of ablation simulation, and 2) obtaining consistent force measurements in the angle-of-attack range from 0° to 4°. The subliming ablator used was camphor, which is compared to transpiration cooling through a porous surface using either sulphur hexafluoride (SF_6), nitrogen, or argon gas. The study shows small differences in data from the two modes of ablation simulation using the sharp 5° cone and indicates that care should be taken in fabricating porous mass-injection models because the mass-injection distribution can have an effect on the measured stability or drag.

Nomenclature

A,B = model dimensions, in. (see Fig. 2)
B_0 = blowing parameter
C_A = forebody axial-force coefficient, $C_{AT}+C_{AB}$
C_{AB} = base axial-force coefficient, $C_{AB}=(p_b-p_\infty)/q_\infty$
C_{AF} = friction axial-force coefficient with blowing, not including viscous interaction
C_{AF_0} = friction axial-force coefficient without blowing, not including viscous interaction
C_{AP} = pressure axial-force coefficient, $p_b=p_\infty$
C_{AT} = total measured axial-force coefficient
C_m = pitching-moment coefficient about a point located at the cone apex, $M/q_\infty S_{\text{ref}} D$
C_N = normal force coefficient, $N/q_\infty S_{\text{ref}}$
C_p = specific heat at constant pressure, Btu/lb°R
D = model diameter, in.
F_i = diffusion factor for species i introduced by the approximation for binary diffusion coefficients[8]
G_i = self-diffusion factor for species i, Eq. (1)[8]
H_e = stagnation enthalpy, Btu/lb
h_w = enthalpy of the edge gas at wall temperature, Btu/lb
k = thermal conductivity, Btu/ft^2-sec-°R
L = total model axial length, in. (Fig. 2)
M = pitching moment about a point located at the cone apex, in.-lb
M_∞ = freestream Mach number
$\dot{m}_w$ = local blowing or ablation rate, psf-sec
N = normal force, lb
p = surface pressure, psia
p_b = base pressure, psia
p_0 = stagnation pressure in reservoir, psia
p_∞ = freestream static pressure, psia
$\dot{q}_w$ = wall heat-transfer rate with blowing, Btu/ft^2-sec
$\dot{q}_{0,w}$ = wall heat-transfer rate without blowing, Btu/ft^2-sec
q_∞ = freestream dynamic pressure, psia
R_B = model base radius, in.
Re_∞ = freestream Reynolds number per foot
$Re_{\infty,L}$ = freestream Reynolds number based on model length
R_N = model nose radius, in.
S = surface area of model, in.^{2}
S_{ref} = reference area, πR_B^2, in.^{2}
S_w = total surface area of model, in.^{2}
T_0 = stagnation temperature, °R
T_w = wall temperature, °R
X = axial distance from apex of model, in.
X_{cg}/L = nondimensional axial distance from model apex to the reference center of gravity (Fig. 2)
X_{cp}/L = nondimensional center of pressure, defined as $(-C_m/C_N)(D/L)+X_{cg}/L$
α = angle of attack, deg
θ_c = cone half-angle, deg

Introduction

THE ablation of re-entry vehicles is a complex process involving interactions between the vehicle heat-shield material and its aerothermodynamic environment, including such phenomena as chemical reactions between the vehicle surface material and the high-temperature air species (including chemical kinetics), mechanical erosion, radiation, vehicle shape change, boundary-layer transition, and the effects of the injection of the ablation gases into the boundary layer. This paper is concerned with the simulation in the wind tunnel of mass injection into the boundary layer and its effects upon vehicle stability and drag.

Mass-injection effects generally are simulated in the wind tunnel by injecting gas through the surface of a porous model. This method of simulation has several advantages over low-temperature ablators (better control of injection rates and test conditions, better data-acquisition rates) and so is an attractive technique. However, an experimental and analytical comparison of transpirationally cooling a model as opposed to using a subliming low-temperature ablator has not been made on an identical model. This paper presents a direct experimental and analytical comparison of the force and moment data of a sharp 5° cone at Mach number of 10 under laminar flow conditions (freestream Reynolds number of 1×10^6/ft) with the two modes of mass injection. The model was fabricated to allow testing with a solid steel, a porous shell, or a camphor sleeve with only minor model configuration changes. In order to separate the influence of

Presented at the AIAA 9th Aerodynamic Testing Conference, Arlington, Texas, June 7-9, 1976 (in bound volume of Conference papers, no paper number); submitted June 24, 1976; revision received April 7, 1977.

Index categories: Entry Vehicle Testing, Flight and Ground; Boundary Layers and Convective Heat Transfer—Laminar; Supersonic and Hypersonic Flow.

*Assistant Branch Manager, Aerodynamics Projects Branch, von Kármán Gas Dynamics Facility, AEDC Division. Associate Fellow AIAA.

†Research Engineer, Aerodynamics Projects Branch, von Kármán Gas Dynamics Facility, AEDC Division. Member AIAA.

‡Lead Engineer, Project Support and Special Studies Section, Aerodynamics Projects Branch, von Kármán Gas Dynamics Facility, AEDC Division. Member AIAA.

molecular weight, a wide range of gases was utilized, specifically, SF_6 (sulphur hexafluoride), argon, and nitrogen, which have molecular weights of 146, 40, and 28, respectively. The molecular weight of the camphor was 152. The model was injected into the tunnel at zero angle of attack for a few seconds and pitched in a continuous-sweep mode to over 3° angle of attack and back to zero at a rate of approximately 1 deg/sec. The camphor model pieces were weighed before and after each run, and the time exposed to the flow was recorded. A sketch showing the sting arrangement of the 5° cone model is shown in Fig. 1.

Apparatus and Procedure

Wind Tunnel

Tunnel C[1] is a closed-circuit hypersonic wind tunnel with a 50-in.-diam test section and an axisymmetric contoured nozzle that provides a nominal Mach number of 10 over a range of pressure levels from 175 to 2000 psia. Stagnation temperatures sufficient to avoid air liquefaction in the test section (up to 2000°R) are maintained at all conditions. The tunnel is equipped with a model injection system, which allows removal of the model from the test section while the tunnel is in operation. For the tests reported here, tunnel C was operated at a stagnation pressure of 700 psia and a reservoir temperature of 1895°R.

Sharp 5° Cone Model

A 5° half-angle cone model, 21 in. long with a 3.68-in. base diameter, was designed and fabricated for these experiments (see Fig. 2). The model was fabricated with an interchangeable steel nose section, rear frustrum, and steel baseplate that permitted testing a solid steel frustrum or camphor frustrum or a porous sintered metal frustrum.

Figure 3 shows the computed distribution of ablation along the camphor surface ($\alpha = 0$) relative to a uniform ablation rate. A gross calibration of the porous frustrum also is given in Fig. 3. The normalized values given at each station represent the measured flow rate at that location on the model surface relative to a calculated flow for uniform blowing. This distribution was measured using a hot-wire probe. It is very difficult to build into a porous model the distribution one would like to have, which is one of the primary disadvantages of this mode of ablation simulation. The influence of this type of distribution on the zero lift axial force can be computed. However, the influence on the static stability of the model is not predicted easily. A laminar boundary layer presumably would be more sensitive to variations in the upstream history of the mass injection than would a turbulent boundary layer.

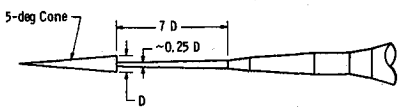

Fig. 1 Schematic of wind-tunnel support arrangement.

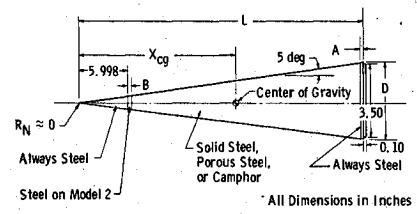

	Configuration	L	X_{cg}	D	X_{cg}/L	A	B
Model 1	Steel or Camphor	21.003	14.219	3.675	0.6770	0.266	0
Model 2	Porous	21.029	14.237	3.680	0.6770	0.188	0.281

Fig. 2 5° sharp cone test model.

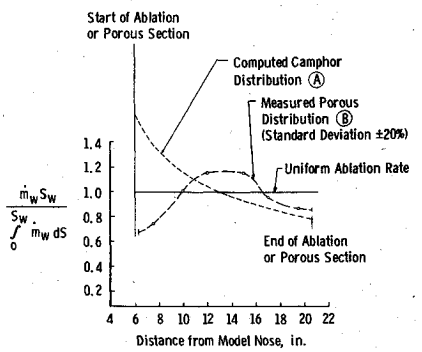

Fig. 3 Relative axial distribution of mass injection for camphor or porous model.

Balance and Data Precision

A special three-compoent force balance was designed and fabricated for this test program. The original design criteria for this balance were as follows: the balance was to measure normal force loads up to 9 lbf to within 0.01 lbf and axial forces up to 1.5 lbf to within 0.003 lbf, and pass mass flow rates up to 0.010 lbm/sec with bellows pressure of less than 200 psia.[2] The mass flow line (a 0.125-in.-o.d. tube) passes through the forward and aft axial members of the balance. The gas supply then enters a small bellows section, and from there passes through ten 0.063-in.-diam holes into a manifold. There is a bellows section on either side of this section of the 0.125-in.-diam gas supply line to minimize the influence of the mass flow system on the balance performance. A water jacket encloses the balance to keep the balance temperature within operational limits.

The balance performance met the original design criteria with the mass flow system disconnected; however, the presence of the gas supply (i.e., pressure in the mass flow line) reduced the balance performance so that the uncertainty in the force measurements increased by a factor of about 5. An overall repeatability of the data from run to run and tunnel entry to tunnel entry is given in Table 1.

Test Techniques

As a result of the nature of the models, the sensitivity of the specially designed balance, and the test requirements, nonstandard test procedures for wind-tunnel force measurements were employed. Since some of the models used in the test programs ablated with time when exposed to an airstream, it was necessary to restrict this time of exposure in the airstream to less than 1 min. The sensitivity of the balance output and the adverse model vibration produced by the tunnel operation required that electrical filters be imposed on the balance electrical responses. Also, the presence of a mass flow or pressurized bellows system in the balance which affected the zeros and repeatability of the balance imposed additional restrictions on the testing technique. Finally, the obvious test requirement to record the maximum amount of useful information including repeat data in the shortest time interval indicated that a continuous-sweep, data-recording mode of operation should be employed.

In the case of the ablative models, the following procedure was adopted in recording the test results. The ablative components of the model were weighed before and after each run; also, an evaluation was made of the time that the model was exposed to the airstream. In addition to weighing the model components, the three-component force balance also

Table 1 Wind-tunnel data repeatability

p_0, psia	C_N	C_m	C_{AT}	C_A
700	±0.0008	±0.0012	±0.001	±0.0018

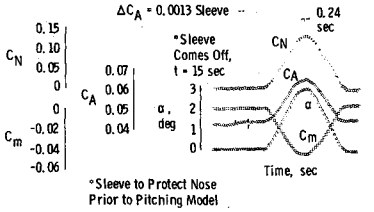

Fig. 4 Data vs time, $R_N/R_B=0.05, \theta_c=4°$.

was used to define the model tare weight before and after each model injection into the tunnel airstream. Once the instrumentation was activated, the model was injected into the tunnel at zero angle of attack and then automatically pitched slowly (about 1 deg/sec) to a maximum angle of 3° to 4° and then back to 0°, and to −1°, and finally returned to zero angle of attack and immediately retracted. A typical run sequence is shown in Fig. 4 for a 4° half-angle cone model run during this same test program but not reported on here. These data are also typical of the 5° half-angle cone model. Note, however, that some of the 4° half-angle cone models did not have a metal nose and were protected during the model injection process with an aluminum sleeve. The effect of the sleeve on the axial force is apparent in the figure. The sleeve was not used on the 5° half-angle cone model.

The same process was used when data were recorded for the porous mass addition and solid stainless-steel model configurations. In the case of the porous models, all model zeros were recorded in the injection tank after the mass flow rate through the model was established and prior to injection of the model into the airstream. These preloading procedures improved the repeatability of the balance zeros and the reliability of the test results.

Test Conditions

All of the experimental data reported here were run at the nominal test conditions given in Table 2.

Theoretical Friction Drag Predictions

Several boundary-layer calculations were made at 0° angle of attack for the ablating camphor wind-tunnel models and for the wind-tunnel models with various gases injected into the boundary layer. The main objective of these calculations was to predict the reduction in friction drag caused by the mass injection. The effects of injecting the different molecular weight gases was studied; and the effect on the friction drag of the different mass-injection distributions was determined theoretically. The Aerotherm Boundary Layer Integral Matrix Procedure (BLIMP) computer program[3-5] was used to obtain these numerical solutions of the nonsimilar laminar boundary layer. A few calculations also were made for "air blowing into air" using the computer program of Adams.[6]

The boundary layer over the wind-tunnel models was laminar. The pressure distribution for the boundary-layer calculations was taken from the sharp cone solutions of Jones[7]; that is, the pressure was taken to be constant over the model surface ($p=0.03818$ psia). The transport properties for the various gas mixtures were modeled in the BLIMP program using approximate relations for viscosity and conductivity of the Sutherland-Wassilijewa type.[8] The diffusion factors F_i and G_i (required inputs for the BLIMP program) were chosen to give the best agreement with published transport property data[9-12] whenever they were available. (No transport property data were available for camphor.) The various gases were injected experimentally at temperatures near 550°R, and the wall temperature was taken to be 550°R over the length of the models for the theoretical predictions, except for the camphor models, where the wall temperature was calculated theoretically ($T_w=530$-550°R).

Table 2 Nominal wind-tunnel test conditions

p_0, psia	T_0, °R	M_∞	Re_∞, ft	T_w, °R
700	1895	10	1×10^6	550

Table 3 Properties of camphor[13-15]

Chemical formula	$C_{10}H_{16}O$
Heat of sublimation	151.36 Btu/lb
C_p (solid or gas)	0.400 Btu/lb-°R
Molecular weight	152.2
Density	62.4 lb/ft^3
k (solid)	3.2×10^{-5} Btu/ft^2-sec-°R

Camphor Model Calculations

The wall boundary conditions for the camphor model runs, specifically the wall temperature and the surface ablation rates, were calculated assuming a steady-state surface energy balance and assuming that the "camphor gas" was in equilibrium with the solid camphor. The camphor properties used for these calculations are given in Table 3 and were taken from Tables 4-1 and 4-2 of Ref. 13 (pp. 4-12 and 4-13). Essentially these same property values are also given by Lippert and Genovese[14] and by Baker.[15] The "camphor-air" mixture was considered to be a nonreacting mixture of "camphor" and "air."

A transient calculation made using the thermal conductivity given in Table 3 indicated that the time to reach 95% of the steady-state ablation rate is 0.2 sec. The camphor transport properties were calculated using the model incorporated in the BLIMP computer program and using diffusion factors F_i and G_i obtained from a correlation[8] in terms of molecular weight, because no experimental data were available.

The overall veracity of the camphor ablation modeling method and the veracity of the camphor property data were checked by comparing the measured model weight loss vs the predicted weight loss for the 5° sharp cone model. Also, theoretical vs experimental camphor ablation rates were compared in the blunt nose region of a 4° half-angle cone model run as a part of the test program but not reported on here.

Mass-Injection Simulation Parameter

The total mass injected into the boundary layer over the entire model is represented by a normalized mass addition parameter defined as follows:

$$B_0=[(H_e-h_w)/S_w(\dot{q}_{0,w})_{x/L=1}]\int_0^{S_w}\dot{m}_w dS$$

where the $\int_0^{S_w}\dot{m}_w(dS/S_w)$ term represents an average mass-injection rate for the model, and where the nonablating heat-transfer rate at the end of the body is used as a normalizing parameter. This B_0 is similar to the commonly used local normalized-mass-addition parameter. For a sharp cone model that is ablating over its entire length with a "camphor-type" mass injection distribution, B_0 would be constant regardless of model scale ($B_0=1.45$ for a sharp 5° half-angle cone model at the conditions of the present test: $p_0=700$ psi, $T_0=1895$°R). The calculated B_0 for the camphor model run during these tests was 1.25, which is a reflection of the fact that there was a nonablating nose section on the model.

Note that this test was run at constant total enthalpy, so that the B_0 variation shown here was obtained by varying the injection rate of the injected gases. It would be necessary to use the adiabatic wall enthalpy instead of the total enthalpy in the B_0 definition in order to correlate data taken over a range of total enthalpies.

Table 4 Comparison of theory and experiment at $\alpha = 0°$ for a nonablating sharp 5° half-angle cone model

	Experiment	Lubard and Helliwell[17]	BLIMP[3]	Adams[6]
Total forebody drag coefficient ($p_b = p_\infty$), C_A	0.0413[a]	0.04076	...	...
Pressure drag coefficient including viscous interaction	...	0.02063	...	...
Friction-drag coefficient including viscous interaction	...	0.02013	...	...
Friction-drag coefficient (no viscous interaction), C_{AF_0}	0.02017[b]	...	0.01963	0.01909
Heat-transfer rate at end of body, $(\dot{q}_{0,w})_{X/L=1}$	...	...	0.0494	0.0494

[a] Base pressure was measured on the zero mass injection run and used to correct the measured drag, C_{AT} to the forebody drag C_A.
[b] Not measured directly, but deduced as described in the text.

Theoretical Results

Experimental data for the no-injection case at zero angle of attack are shown in Table 4, along with several theories. Theoretical results are shown from the BLIMP[3] program, from Adams,[6] and also calculations of Adams and Griffith[16] using the hypersonic viscous shock layer approach of Lubard and Helliwell.[17] The Lubard-Helliwell results include viscous interaction effects, but the BLIMP results and Adams' results do not. The magnitude of the viscous interaction effects may be estimated by taking the difference between the Lubard-Helliwell results and the pressure-drag coefficient and friction-drag coefficient determined by methods that do not include these effects. This was done was follows:

$$\Delta C_{AP} = 0.02063 - 0.0188 = 0.00183$$

where the pressure drag coefficient without viscous interaction (0.0188) was taken from Jones,[7] and

$$\Delta C_{AF_0} = 0.02013 - 0.01963 = 0.0005$$

where the friction-drag coefficient without viscous interaction was taken from the BLIMP results.[3] It is recognized that some of the increments are caused by the difference in the method of calculation rather than by viscous interaction, but this was the only method of estimation available, and the total viscous interaction effect is small (0.00233). In deducing friction-drag values from the experimental data, the pressure drag coefficient of Jones[7] and the total viscous-interaction drag coefficient just given were subtracted from the experimental forebody drag coefficients, regardless of whether or not there was mass injection ($C_{AF} = C_A - 0.0188 - 0.00233$). This neglects any effect of viscous interaction due to mass injection.

It may be seen in Table 4 that there is excellent agreement between the experimental data and the theory of Lubard-Helliwell[17] for the total forebody drag coefficient, and that there is very reasonable agreement between the experimentally deduced friction drag and the BLIMP[3] results (2%) and Adams[6] results (5%). The values of C_{AF_0} given in the table were used to nondimensionalize the friction drag for several figures presented below. Also, the value of $(\dot{q}_{0,w})_{X/L=1} = 0.0494$ Btu/ft^2-sec was used in the blowing parameter B_0.

Theoretical results for the reduction in friction drag due to injecting either nitrogen or SF_6 gases are presented in Fig. 5 for a range of B_0's. For each of the injected gases, calculations were made with the two different mass-injection rate distributions previously shown in Fig. 3, i.e., for the mass-injection rate distribution for the transpiration-cooled model run during these tests, and for the mass-injection rate distribution for the camphor models run during these tests. B_0 was varied for these calculations by varying the mass-injection rates and keeping the other parameters constant

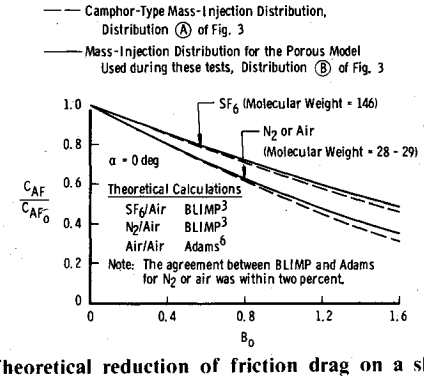

Fig. 5 Theoretical reduction of friction drag on a sharp 5° cone caused by mass injection.

(H_e, h_w, p_0, model size). This is also the way that B_0 was varied during the experiments for the transpiration-cooled model. B_0 was kept essentially constant for the camphor model experiments.

As expected, there is considerably less reduction in the friction drag whenever the heavier SF_6 gas is injected as compared to nitrogen gas injection at the same B_0. It is interesting to note that the viscosity at the wall actually was smaller for the SF_6-air mixture than it was for the N_2-air mixture, and that the wall velocity gradient therefore was considerably larger for the SF_6-air mixture. It also is of interest to observe that at the high B_0's the local skin-friction drag coefficients at the end of the body were over a factor of 4 higher in the case of SF_6 gas injection compared to N_2 gas injection, although the integrated value over the whole body was only 50% higher.

There is a definite effect of the mass-injection distribution on the skin-friction drag reduction due to blowing, with the camphor-type distribution giving the larger reduction in skin-friction drag. Excellent agreement was obtained between the BLIMP theoretical calculations (N_2/air) and those of Adams (air/air).

Results and Discussion

Transpiration Experiments (SF_6, Ar, N_2)

Selected basic data for the transpirational cooling experiments are given in Figs. 6 and 7 for SF_6 and nitrogen. The data for zero blowing were taken using model 1 (Fig. 2) in order to keep the porous sintered metal from being exposed to the high stagnation temperature of tunnel C without surface cooling. Injecting SF_6 through the surface of model 2 (Fig. 2) moves the center of pressure forward, decreases the normal-force coefficient, and decreases the axial force (see Fig. 6). The decrease in normal force probably is caused by higher surface pressures on the lee side of the model because of

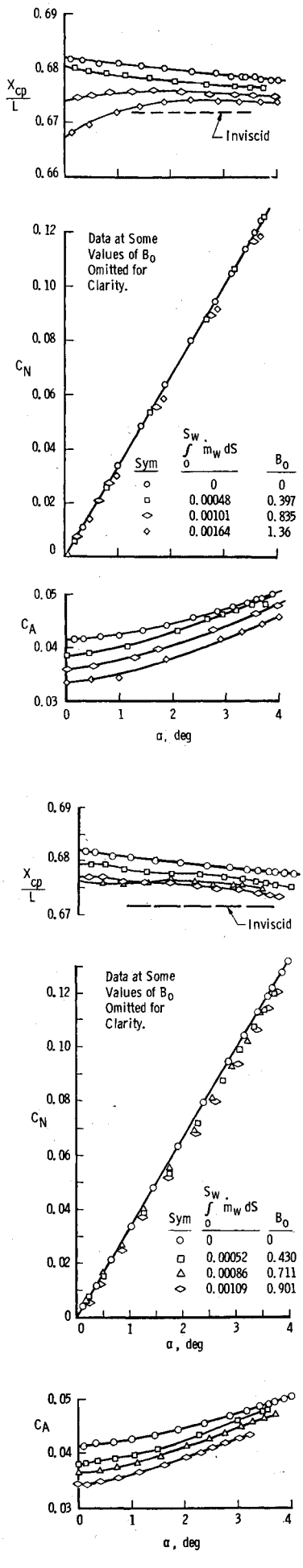

Fig. 6 Basic data for SF_6 blowing.

Fig. 7 Basic data for nitrogen blowing.

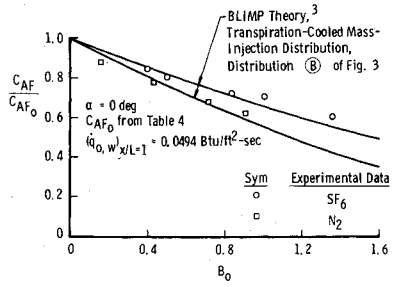

Fig. 8 Comparison of experimental vs theoretical friction-drag reduction caused by blowing SF_6 or nitrogen.

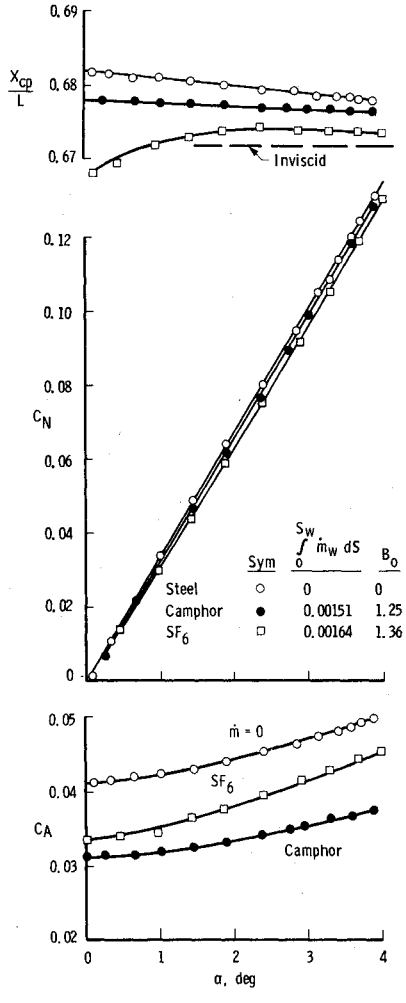

Fig. 9 Comparison of camphor ablation and SF_6 blowing.

blowing. The reduction in axial force is caused by the lower model friction drag. The forward movement in the center of pressure may be caused partly by reducing the friction drag of the model, since viscous effects tend to move the center of pressure aft on the model.

Figure 7 presents the data with nitrogen blowing. The trends are very similar to the SF_6 results, indicating a weak influence of molecular weight on the drag and static stability of the model caused by blowing. The argon results were similar and are not shown.

A comparison is given in Fig. 8 of the experimental friction-drag reduction due to blowing with the theoretical reduction predicted using the BLIMP[3] computer program ($\alpha = 0$). The comparison is quite good. The general trend of the measured reduction of friction drag with increased mass injection for either gas injectant is predicted reasonably, as is the general trend for the effect of injecting different molecular weight gases.

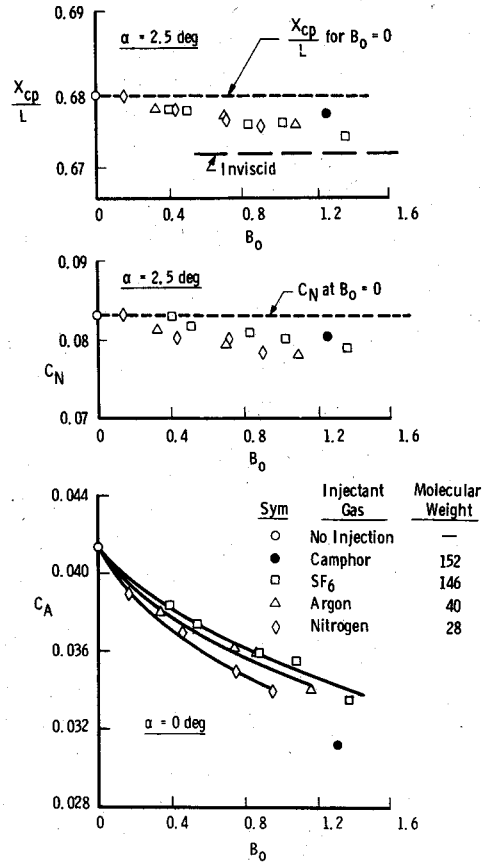

Fig. 10 Summary of the effects of blowing various injectants.

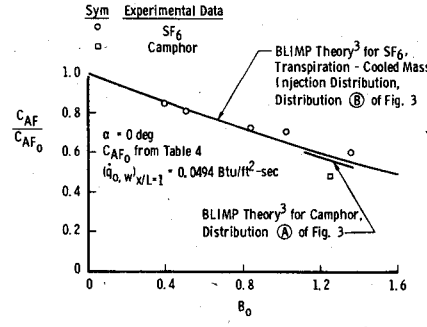

Fig. 11 Friction-drag reduction on a sharp 5° cone model: SF_6 blowing vs camphor ablation.

Camphor Ablation and Comparisons

The effect of camphor ablation on the 5° sharp cone is shown in Fig. 9. Data for SF_6 injection at a similar blowing rate also are shown, so that a direct comparison can be made between the two modes of ablation simulation. Camphor ablation causes a greater reduction in C_A, especially at angle of attack, and only a slight forward shift in the center of pressure. It is likely that at least part of the difference is caused by the different mass-injection distributions.

A summary of the effect of the two modes of ablation simulation is presented in Fig. 10 over a range of the blowing parameter B_0. The zero-angle-of-attack axial-force data show a definite trend with molecular weight. The normal force is reduced in a similar manner by all three of the injected gases and also by the camphor ablation. The molecular weight of the injected gas has no significant influence on the amount of the forward center-of-pressure shift, and the mode of ablation has only a slight effect, as noted.

Figure 11 presents a comparison of the experimental reduction in friction drag at zero angle of attack for the porous model with SF_6 blowing and for the camphor ablating model, along with the theoretical predictions of these mass-injection effects. From a theoretical point of view, injecting the same amount (same B_0) of either SF_6 or camphor makes little difference. Both gases have about the same molecular weight, were injected at about the same T_w, and should have about the same viscosity and thermal conductivity. (No published data for camphor were found.) The theoretical difference in friction-drag reduction due to injecting SF_6 as opposed to camphor virtually all can be attributed to the differences in the mass injection distributions (see Fig. 5). The theoretical friction-drag reduction due to camphor ablation falls on top of the curve in Fig. 5 given for SF_6 injected with a "camphor-type" mass injection distribution. Experimentally, there is an additional reduction in friction drag with camphor ablation beyond that due to the different mass-injection distributions and beyond that predicted theoretically.

Summary

Results of the research are summarized as follows:

1) A direct comparison between a model utilizing transpiration cooling with sulphur hexafluoride and one using a subliming low-temperature ablator (camphor) reveals small but significant differences in the moment and drag characteristics for a 5° half-angle cone with a sharp nose. It was shown theoretically for the zero-angle-of-attack drag data that part of the difference was due to the different mass-injection distributions. The reason for the remaining differences is not known. Care should be taken with the fabrication of porous injection models because the effect of the mass-injection distribution could be important.

2) Mass injection using camphor is more effective in reducing the laminar friction drag of the sharp 5° cone than is blowing through a porous surface using any of the injected gases (N_2, Ar, or SF_6), especially at angle of attack ($\alpha < 4°$).

3) The center of pressure (X_{cp}/L) moves forward on the model with either transpiration cooling or camphor ablation. No effect of molecular weight is noted in the X_{cp}/L movement. Camphor ablation results in a 0.2% forward movement at $B_0 = 1.25$, whereas transpiration cooling shifts the X_{cp}/L about 0.4%.

4) The normal-force coefficient is decreased slightly (about 4% at $B_0 = 1.25$) with both transpiration cooling and camphor ablation.

5) The theoretical calculations at 0° angle of attack are generally in good agreement with the experimental results, except for the previously noted disagreement for the camphor ablation results.

Acknowledgment

The work reported herein was conducted by Arnold Engineering Development Center (AEDC), Air Force Systems Command (AFSC). The work was performed by ARO, Inc. (a Sverdrup Corporation Company), contract operator of AEDC.

References

[1] "von Kármán Gas Dynamics Facility, Vol. 3," *Test Facilities Handbook*, 10th Ed., Arnold Engineering Development Center, Arnold Air Force Station, Tenn.

[2] Griffith, B.J., Strike, W.T., and Majors, B.M., "Ablation and Viscous Effects on the Force and Moment Characteristics of Slender Cone Models at Mach 10 under Laminar Flow Conditions," Arnold Engineering Development Center, Arnold Air Force Station, Tenn., AEDC-TR-75-109, Oct. 1975.

[3] Kendall, R.M. and Bartlett, E.P., "Nonsimilar Solution of the Multicomponent Laminar Boundary Layer by an Integral-Matrix Method," *AIAA Journal*, Vol. 6, June 1968, pp. 1089-1097.

[4] Anderson, L.W. and Kendall, R.M., "A Nonsimilar Solution for Multicomponent Reacting Laminar and Turbulent Boundary Layer Flows Including Transverse Curvature," Air Force Weapons Lab., Kirtland Air Force Base, N.Mex., AFWL TR-69-106, March 1970.

[5] Bartlett, E.P., Kendall, R.M., and Rindal, R.A., "A Unified Approximation for Mixture Transport Properties for Muiticompoent

Boundary Layer Applications," Aerotherm Corp., Mountain View, Calif., Rept. 66-7, Pt. IV, March 1967.

[6] Adams, J.C., Jr., "Eddy Viscosity-Intermittency Factor Approach to Numerical Calculation of Transitional Heating on Sharp Cones in Hypersonic Flow," Arnold Engineering Development Center, Arnold Air Force Station, Tenn., AEDC-TR-70-210, (AD714058), Nov. 1970.

[7] Jones, D.J., "Tables of Inviscid Supersonic Flow about Circular Cones at Incidence, $\gamma = 1.4$, Parts I and II," AGARDograph 137, Nov. 1969.

[8] Deblaye, C. and Bartlett, E.P., "An Evaluation of Thermodynamic and Transport Properties for Use in the BLIMP Nonsimilar Multicomponent Boundary-Layer Program," Sandia Labs., Rept. SC-CR-69-3271, July 1969.

[9] Svehla, R.A., "Estimated Viscosities and Thermal Conductivities of Gases at High Temperatures," NASA TR R-132, 1962.

[10] McCoubrey, J.C. and Singh, N.M., "Intermolecular Forces in Quasi-Spherical Molecules," *Transactions of the Faraday Society,* Vol. 53, Pt. 7, July 1957, pp. 877-883.

[11] Ellis, C.P. and Raw, C.J.G., "High-Temperature Gas Viscosities. II: Nitrogen, Nitric Oxide, Boron Trifluoride, Silicon Tetrafluoride, and Sulfur Hexafluoride," *The Journal of Chemical Physics,* Vol. 30, Feb. 1959, pp. 574-576.

[12] Ames Research Staff, "Equations, Tables, and Charts for Compressible Flow," NACA Rept. 1135, 1953.

[13] Derbidge, T.C., Wool, M.R., Morse, H.L., and Overly, P.T., "Interim Report, Passive Nosetip Technology (PANT) Program," Air Force Space and Missile Systems Organization, Los Angeles, Calif., SAMSO-TR-74-86, Vol. V, Pt. III, Jan. 1974.

[14] Lippert, F. and Genovese, J., "An Experimental Study of the Boundary Layers on Low-Temperature Subliming Ablators," *AIAA Journal,* Vol. 9, July 1971, pp. 1330-1337.

[15] Baker, R.L., "Low Temperature Ablator Nosetip Shape Change at Angle of Attack," AIAA Paper 72-90, San Diego, Calif., Jan. 1972.

[16] Adams, J.C., Jr. and Griffith, B.J., "Hypersonic Viscous Static Stability of a Sharp 5-Deg Cone at Incidence," *AIAA Journal,* Vol. 14, Aug. 1976, pp. 1062-1068.

[17] Lubard, S.C. and Helliwell, W.S., "Calculation of the Flow on a Cone at High Angle of Attack," R&D Associates, Santa Monica, Calif., RDA-TR-150, Feb. 1973; also *AIAA Journal,* Vol. 12, July 1974, pp. 965-974.